

# Exploiting Dynamic Opening of Apertures in a Partially Fluorinated MOF for Enhancing H<sub>2</sub> Desorption Temperature and Isotope Separation

Linda Zhang,<sup>†,◇</sup> Seohyeon Jee,<sup>‡,◇</sup> Jaewoo Park,<sup>§</sup> Minji Jung,<sup>§</sup> Dirk Wallacher,<sup>||</sup> Alexandra Franz,<sup>||</sup> Wonjoo Lee,<sup>⊥</sup> Minyoung Yoon,<sup>#,Ⓛ</sup> Kyungmin Choi,<sup>\*,‡,Ⓛ</sup> Michael Hirscher,<sup>\*,†,Ⓛ</sup> and Hyunchul Oh<sup>\*,§,∇,Ⓛ</sup>

<sup>†</sup>Max Planck Institute for Intelligent Systems, Heisenbergstraße 3 70569 Stuttgart, Germany

<sup>‡</sup>Department of Chemical and Biological Engineering, Sookmyung Women's University, 100 Cheongpa-ro 47 gil, Yongsan-gu, Seoul 04310, Republic of Korea

<sup>§</sup>Department of Energy Engineering, Gyeongnam National University of Science and Technology (GNTECH), Jinju 52725, Republic of Korea

<sup>||</sup>Helmholtz-Zentrum Berlin für Materialien und Energie GmbH, 14109 Berlin, Germany

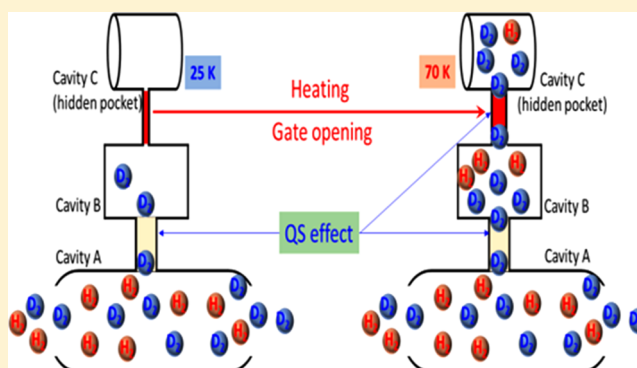
<sup>⊥</sup>Department of Defense Ammunitions, Daeduk College, Daejeon 305-715, Republic of Korea

<sup>#</sup>Department of Chemistry, Kyungpook National University, Daegu 41566, Republic of Korea

<sup>∇</sup>Future Convergence Technology Research Institute, Jinju 52725, Republic of Korea

## Supporting Information

**ABSTRACT:** Deuterium has been recognized as an irreplaceable element in industrial and scientific research. However, hydrogen isotope separation still remains a huge challenge due to the identical physicochemical properties of the isotopes. In this paper, a partially fluorinated metal–organic framework (MOF) with copper, a so-called FMOFCu, was investigated to determine the separation efficiency and capacity of the framework for deuterium extraction from a hydrogen isotope mixture. The unique structure of this porous material consists of a trimodal pore system with large tubular cavities connected through a smaller cavity with bottleneck apertures with a size of 3.6 Å plus a third hidden cavity connected by an even smaller aperture of 2.5 Å. Depending on the temperature, these two apertures show a gate-opening effect and the cavities get successively accessible for hydrogen with increasing temperature. Thermal desorption spectroscopy (TDS) measurements indicate that the locally flexible MOF can separate D<sub>2</sub> from an isotope mixture efficiently, with a selectivity of 14 at 25 K and 4 at 77 K.



## INTRODUCTION

Deuterium, the stable hydrogen isotope, has been recognized as an irreplaceable element in industrial and scientific research, used in neutron scattering techniques, in nonradioactive isotope tracing, and as a fuel source for nuclear fusion reactors.<sup>1</sup> Thus, a reliable source of high-purity deuterium is indispensable for those industrial applications. However, deuterium enrichment remains problematic because of the extremely low abundance of this stable hydrogen isotope, as well as the nearly identical physicochemical properties of hydrogen isotopes.<sup>2</sup> Currently, only a limited number of large-scale techniques have been used for industrial purification of the heavy hydrogen isotope, such as electrolysis of heavy water extracted via the Girdler-sulfide process, or cryogenic distillation, which is performed at 24 K. However, both methods tend to be extremely time consuming and energy

intensive, with low separation efficiencies (2.3 and 1.5, respectively).<sup>3</sup> Generally, molecular sieves are often utilized in industry for purification of gas mixtures with different molecular size. However, in contrast to conventional gas mixture separation, special efforts are required in hydrogen isotope separation due to their shape and identical kinetic diameter. The separation can be realized by a promising alternative using nanoporous materials on the basis of their preference for heavier isotopes via kinetic quantum sieving (KQS).<sup>4</sup> KQS takes place in a system where the difference between the pore size and molecular size becomes comparable to the de Broglie wavelength under cryogenic conditions.<sup>5</sup> In this confinement, the lighter isotope encounters a greater

Received: September 23, 2019

Published: November 21, 2019

diffusion barrier due to the higher zero-point energy (ZPE). Thus, deuterium can diffuse more quickly than hydrogen inside the porous materials, resulting in the separation of the isotopes. Therefore, the aperture size plays an important role in isotope separation. The KQS phenomenon has been experimentally investigated in various porous materials, including carbons,<sup>6,7</sup> zeolites,<sup>7,8</sup> covalent organic frameworks (COFs),<sup>9</sup> and metal–organic frameworks (MOFs).<sup>10,11</sup> Especially the last two, COFs and MOFs, with exceptional surface area and tunability of pore size and functionality, have recently received increasing attention for possible applications in isotope separation of light gases.<sup>9–16</sup> Fundamental studies have been carried out on the correlation between KQS and pore aperture size in porous materials to optimize the separation performance. Chen et al. observed experimentally kinetic isotope quantum sieving at 77 K in narrow pores <5.6 Å.<sup>15</sup> Oh et al. reported the optimal diameter of the aperture should lie in the range 3.0–3.4 Å in rigid frameworks under cryogenic conditions.<sup>16</sup> However, due to the weak binding energies of hydrogen isotopes on the inner surface of porous materials, a high separation performance can only be observed at near zero-coverage pressure, which is not suitable for practical application. To enhance the operating pressure, porous materials with flexible structure and dynamic properties have emerged as good candidates.<sup>17–20</sup> MIL-53 has been reported by Kim et al. to effectively separate hydrogen isotopes, benefiting from its breathing behavior of dynamic pore aperture.<sup>21,22</sup> By tuning of the pore state of this flexible MOF, the highest D<sub>2</sub> over H<sub>2</sub> selectivity of 13 was reached at 40 K.<sup>6</sup> Interestingly, the operating conditions can be enhanced not only by typical flexible frameworks, where a volume or phase change occurs, but also via structures whose flexibility originates from local deformations or vibrations. A temperature-triggered gate-opening induced isotope separation was reported by Oh et al.<sup>9</sup> in the flexible pyridine-decorated COF-1. The highest selectivity was 9.7, observed at 26 mbar and 22 K, which could be ascribed to the quantum isotope effect with cryogenic flexibility. Another temperature-triggered gate opening was found by Teufel et al.<sup>23</sup> in MFU-4, possessing a bimodal pore structure with alternating small and large cavities connected by narrow aperture (ca. 2.5 Å) formed by Cl atoms. Due to phonon-induced vibrations of the Cl atoms at the aperture, hydrogen isotopes (ca. 2.89 Å) could only penetrate into the internal pores at higher temperatures, resulting in a high selectivity of 7.5 at 60 K. Additionally, this gating effect will allow access to the inner surface of the large cavity, which increases the total gas uptake above the opening temperature. Thus, it is evident that the hydrogen isotope separation performance can be improved by introducing local flexibility (or dynamic opening of the aperture) in the unique bimodal pore structure. In this regard, fluorinated metal–organic frameworks (FMOFs) have emerged as good candidates for enhancing the selective gas adsorption owing to their fluorine-specific properties and unique topologies.<sup>24</sup> Cheetham et al.<sup>25</sup> found an enhanced enthalpy of H<sub>2</sub> adsorption in a three-dimensional fluorinated MOF due to the existence of fluorine atoms exposed on the pore surface, which is comparable to MOFs with coordinately unsaturated metal centers. The increase in the number of fluorine atoms in FMOF, reported by Bu et al.,<sup>26</sup> resulted in a higher H<sub>2</sub> and CO<sub>2</sub> adsorption capacity. Omary et al.<sup>27</sup> reported high-density gas uptake and a unique hysteretic sorption of H<sub>2</sub> within the bimodal structured FMOF1. The enhanced H<sub>2</sub> adsorption can be attributed to the

sequential filling of the multiple gas sorption sites in both small and large pores as well as the resulting remarkable swelling of these framework cavities. Pan et al.<sup>28</sup> reported another fluorinated MOF, MMOM1, containing bimodal channels featuring small windows and large cages. The internal surfaces of MMOM1 had been easily modified by changing the channel curvature to enhance H<sub>2</sub>–sorbent interactions. On the same MOF, Fernandez et al.<sup>29</sup> showed that, for the first time, Kr can be removed from Xe mixtures, owing to the bimodal structure and the temperature-triggered gating effect of a partially fluorinated MOFCu and MOFZn. Thus, partially fluorinated MOFs have potential applications in gas storage and separation due to their unique features.

Herein, we report a hydrogen isotope separation strategy using a partially fluorinated MOF(Cu), FMOFCu, with an alternating small and large cavity structure forming a 1-D channel, accompanied by a hidden pocket blocked by fluorinated windows. The separation performance under different conditions (exposure temperature, pressure, and time) was investigated by low-pressure high-resolution isotherm measurements and cryogenic thermal desorption spectroscopy. Our results clearly show that this trimodal pore structure possessing two bottleneck apertures of 3.6 and 2.5 Å exhibits a gate-opening effect, and these cavities become accessible for hydrogen (or adjustable for aperture size) with increasing temperature. The generated effective pore aperture optimizes the KQS effect, leading to a high selectivity of ca. 14 at 25 K. Moreover, owing to the local flexibility, the hidden pockets become accessible at high temperature. Therefore, the isotope separation performance can be also expected even at high temperatures of 100 K, without the existence of open metal sites. This is a breakthrough, since hardly any MOFs exhibit such a high sorption temperature based on KQS.

## ■ EXPERIMENTAL SECTION

**Preparation of FMOFCu.** FMOFCu was prepared by a hydrothermal synthesis as previously reported.<sup>30</sup> Copper nitrate trihydrate (Cu(NO<sub>3</sub>)<sub>2</sub>·3H<sub>2</sub>O; 0.024 g, 0.1 mmol, Sigma-Aldrich) and 2,2-bis(4-carboxyphenyl)hexafluoropropane (CPHFP; 0.122 g, 0.31 mmol, TCI) were dissolved in deionized water (5 mL) and reacted in a hydrothermal reactor at 150 °C for 12 h. The molar ratio of the reaction was 1:3:2776. The product was repeatedly washed with DMF (10 mL, Aldrich) and methanol (10 mL, SAMCHUN) and dried in a vacuum oven at room temperature.

**Characterization.** The surface morphology and particle size were examined using a scanning electron microscope (JEOL, JSM-7600F). Differential thermal analysis (DTA) and thermogravimetry (TG) were carried out to study the thermolysis process and phase transformation using a simultaneous thermal analyzer (SINCO, TGA 4000). Samples were heated at a rate of 5 °C/min. Powder X-ray diffraction (XRD) was performed on a diffractometer (D8 Advance, Bruker AXS) with Cu K $\alpha$  radiation, and a Bragg–Brentano focusing geometry was employed. Diffractograms were collected in the 5–45° 2 $\theta$  range with a step size of 0.01°. Fourier transform infrared spectroscopy (FT-IR) was carried out on a Thermo Fisher Scientific Nicolet IS50 spectrometer. Samples were analyzed for ATR diamond mode measurement and 60 scans with a resolution of 4 cm<sup>-1</sup>. Spectra were recorded in transmission mode.

**Gas Adsorption Experiment.** A fully automated Sieverts apparatus (Autosorb-iQ2, Quantachrome Instruments) was used to perform the cryogenic adsorption experiments. The calibration cell was an empty analysis carried out at the same temperature and pressure range of each experiment; corrections relating the sample volume and the nonlinearity of the adsorbate were made. Around 50 mg of the sample was activated at 400 K under vacuum for 12 h in order to remove any solvent molecules. A coupled cryocooler based

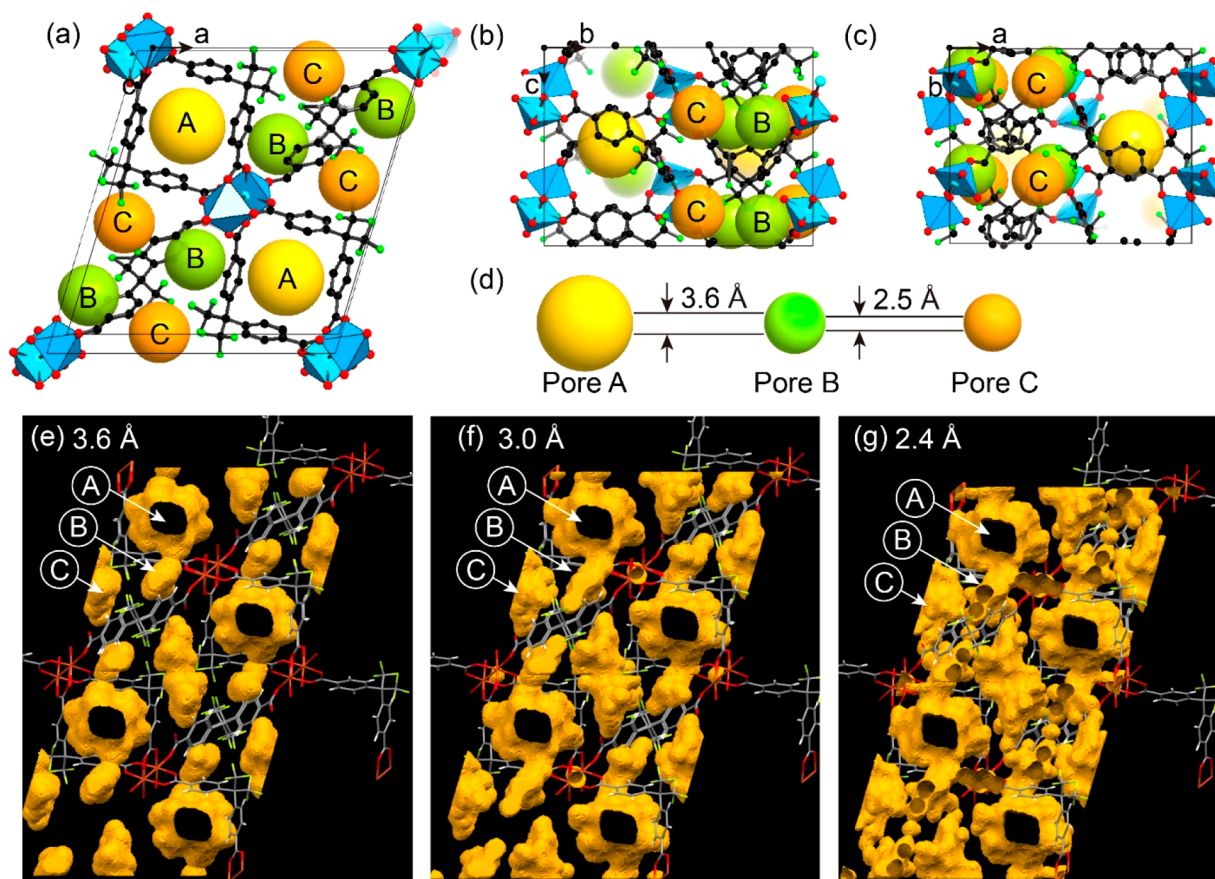


**Figure 1.** Unit cell (a–c) and crystal structure (e–g) of FMOFCu. The yellow, green, and brown spheres represent the volume of pores A, B, and C, respectively. (a) *ac* plane, (b) *bc* plane, and (c) *ab* plane of the unit cell structure. (e–g) Pore network analysis with a grid space of 0.1 Å for the probe sphere. Three cavities (A, B, C) can be identified and are connected depending on the probe size. Pink, red, gray, and blue represent copper, oxygen, carbon, and fluorine atoms, respectively.

on the Gifford–McMahon cycle was used to control the sample temperature. The cooling system permitted us to measure temperatures from 20 to 300 K with a temperature stability of <0.05 K.

**TDS Studies of Hydrogen Isotope Separation.** The selective adsorption after exposure to  $D_2/H_2$  isotope mixtures was directly measured by the setup designed in house for thermal desorption spectroscopy (TDS). For a typical process, about 3.5 mg of a sample was loaded in the sample holder and activated at 400 K under vacuum for 10 h. Then, an equimolar  $D_2/H_2$  isotope mixture was loaded on the sample at a fixed temperature (exposure temperature,  $T_{exp}$ ) for a chosen exposure time ( $t_{exp}$ ). The free gas was evacuated, and then the sample was cooled to 20 K in order to preserve the adsorbed state. Finally, during heating from 20 K to room temperature with a heating rate of 0.1 K/s, the desorbing gas was continuously detected using a quadrupole mass spectrometer (QMS), recognizing a pressure increase in the sample chamber when the gas was desorbed. The area under the desorption peak was proportional to the desorbed amount of gas, which could be quantified after careful calibration of the TDS apparatus.<sup>23</sup>

**Single-Crystal X-ray Structure Analysis.** Crystallographic data for FMOFCu:  $[Cu_2(C_{17}H_8O_4F_6)_2 \cdot (C_{17}H_{10}O_4F_6)]_n$ , FW = 1299.80 g/mol, rod, blue,  $0.038 \times 0.009 \times 0.009$  mm<sup>3</sup>,  $T = 100(2)$  K, monoclinic, space group  $P2_1/n$ ,  $a = 18.707(4)$  Å,  $b = 14.444(3)$  Å,  $c = 20.483(4)$  Å,  $\beta = 106.72(3)^\circ$ ,  $V = 5301(2)$  Å<sup>3</sup>,  $Z = 4$ ,  $D_c = 1.629$  g/cm<sup>3</sup>,  $\mu = 1.499$  mm<sup>-1</sup>,  $F(000) = 2592$ , GOF = 1.065. Of the 28365 reflections, 8255 were unique ( $R_{int} = 0.0791$ ), 5059 observed [ $I > 2\sigma(I)$ ], which refined to  $R_1 = 0.0748$ ,  $wR_2 = 0.1710$ , and for all data  $R_1 = 0.1166$ ,  $wR_2 = 0.1975$ . A single crystal of FMOFCu was coated with Paratone-N oil, and the diffraction data were measured by synchrotron radiation ( $\lambda = 0.8500$  Å) on an ADSC Quantum-210 detector at 2D SMC with a silicon (111) double-crystal

monochromator (DCM) at the Pohang Accelerator Laboratory (PAL; Pohang, Korea). The ADSC Q210 ADX program<sup>31</sup> was used for data collection (detector distance of 63 mm,  $\omega$  scan;  $\Delta\omega = 1^\circ$ , exposure time of 4 s per frame), and HKL2000sm (version 703r)<sup>32</sup> was used for cell refinement, reduction, and absorption correction. The crystal structure was solved by direct methods using SHELXT (2018/3)<sup>33</sup> for the MOF and refined by full-matrix least-squares refinement using the SHELXL (2018/3)<sup>34</sup> computer program. The positions of all non-H atoms were refined with anisotropic displacement factors. All H atoms were placed using a riding model, and their positions were constrained relative to their parent atoms using the appropriate HFIX command in SHELXL-2018. X-ray diffraction data for the molecule were collected using a synchrotron (PAL). Supplementary crystallographic data for this study is found in CCDC-1944259. The data can be obtained free of charge from [www.ccdc.cam.ac.uk/conts/retrieving.html](http://www.ccdc.cam.ac.uk/conts/retrieving.html) (or from the CCDC, 12 Union Road, Cambridge CB2 1EZ, UK; fax + 44 1223 336033; e-mail [deposit@ccdc.cam.ac.uk](mailto:deposit@ccdc.cam.ac.uk)).

**In Situ Gas Adsorption Neutron Powder Diffraction.** In situ neutron powder diffraction experiments were performed at the E9 diffractometer of Helmholtz Centre Berlin for Materials and Energy. A sample cell made with aluminum alloy was used due to its small cross-section for neutron scattering. Around 200 mg of the sample was activated at 400 K under vacuum for 12 h in order to remove any solvent molecules. Deuterium was used as an adsorption gas in order to minimize the large incoherent neutron scattering cross-section of hydrogen that contributes to signal background. Diffraction patterns were collected for 16 h at  $D_2$  gas loading at 24 K. Radiation with a wavelength of 2.816 Å was chosen for the data collection.

## RESULTS AND DISCUSSION

FMOFCu was successfully synthesized on the basis of a previously reported procedure.<sup>30</sup> FMOFCu has a 3D 2-fold interpenetrating structure containing ordered 1D channels built on Cu<sub>2</sub> paddlewheels. Each paddlewheel unit connects to four adjacent paddlewheel units via the four carboxylate groups of CPHFP ligands to form a 2D network. Because of the bent shape of the ligand (average angle 110°), the 2D network has a wavy sheet structure, which has a 1D porous channel. The 2D network structure was further expanded into a 3D framework structure by connecting the 2D network using H<sub>2</sub>CPHFP (ligand angle 102°), which has a framework construction mode similar to that of a pillared square grid net structure.<sup>35</sup> It should be noted that the connection of 2D layers allows the generation of new hidden cavities surrounded by fluorine atoms. Therefore, this porous material exhibits a unique bimodal pore structure, where the tubular cavities are connected through small cavities with a fluorinated environment.<sup>27</sup> Furthermore, the H<sub>2</sub>CPHFP connects 2D layers by coordinating the axial position of the paddlewheel without deprotonating the carboxylic acid; the bonding is much weaker (bond distance 2.204 Å) than that of the ligands on equatorial positions (bond length 1.958 Å) which can give flexibility as reported by others.<sup>36</sup> In this work, as the as-synthesized product has been washed with distilled water; the two excess CPHFP ligands remain and generate a pillar connecting the adjacent Cu centers.

The crystal structure of FMOFCu (Figure 1) was obtained by a single-crystal XRD analysis. The unique structure contains a trimodal pore system with larger tubular cavities A (9.4 × 9.2 Å<sup>2</sup>) and B (5.6 × 4.2 Å<sup>2</sup>) connected by a small aperture of diameter 3.6 Å, and additionally a third hidden cavity C (8.8 × 4.7 Å<sup>2</sup>) connected to the two tubular cavities by a 1D narrow channel consisting of fluorinated windows with a 2.5 Å wide aperture. On the basis of this structure, the pore network was analyzed with Mercury<sup>37</sup> software using a step size of 0.1 Å for the probe spheres. For a 3.6 Å effective probe size, cavities A and B are already connected while cavity C is completely isolated from the channel. However, when the effective probe size decreases to 2.6 Å, cavity C starts to get connected with cavity B and the channel (Figure 1, Figure S1, and Scheme S1). Please note again that cavity A is solely connected to cavity B through a small window of size 3.6 Å, while cavity C is connected to cavity B by an even smaller window of size 2.5 Å, which can be accessed by gas only if the temperature is high enough, allowing thermal flexibility of the aperture.

The SEM image (Figure S2) reveals a well-spread whisker morphology. The TGA data (Figure S3) show a weight loss of 4.6% between 30 and 250 °C, corresponding to the loss of water molecules. The XRD pattern also presents a well-defined peak (see Figure S4), which matches the simulated pattern, indicating the formation of pure crystalline FMOFCu. The FT-IR spectra (Figure S5) of FMOFCu and CPHFP show peaks in the 1000–1400 cm<sup>-1</sup> region, confirming the presence of C–F groups in both samples. The band observed in the 2500–3300 cm<sup>-1</sup> region in CPHFP is due to O–H stretching in the carboxylic group and shifted to the 3200–3750 cm<sup>-1</sup> region in FMOFCu, indicating the existence of loosely bound water molecules. Gas sorption measurements performed on FMOFCu possessing a bottleneck window (3.6 and 2.5 Å) show that neither N<sub>2</sub> at 77 K nor H<sub>2</sub> at 20 K can penetrate this partially fluorinated MOF due to the comparable size of the

aperture and the kinetic diameter of probe molecules (3.64 Å, N<sub>2</sub>; 2.89 Å, H<sub>2</sub>) (Figure S6).

The low-pressure H<sub>2</sub> sorption isotherms obtained at various temperatures (20–120 K) clearly show the unique sorption behavior of FMOFCu, as shown in Figure 2 (for additional

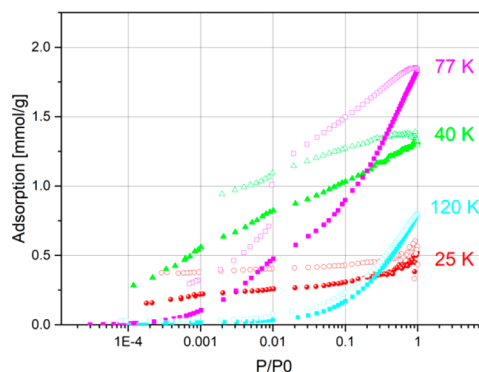


**Figure 2.** Isotherms for H<sub>2</sub> adsorption (closed) and desorption (open) on FMOFCu at various temperatures (25–120 K) in the pressure range 0–1 bar. For isotherms collected at other temperatures, see Figures S7 and S8 in the Supporting Information.

isotherms see Figure S7). Unlike a typical characteristic isotherm (higher uptake with decreasing *T*), hydrogen uptake on FMOFCu starts at 25 K, exhibiting a hysteresis and reaching the maximum uptake at 77 K (1.85 mmol/g at 1 bar). The observed hysteresis becomes stronger in the temperature range up to 77 K and then becomes weaker above 87 K, implying a better equilibrium at higher temperatures. With a further increase in temperature, the gas uptake decreased as in typical sorption isotherms. This unique (inverse) sorption behavior of FMOFCu below 77 K can be ascribed to a strong diffusion limitation, produced by the two small bottleneck windows, which does not allow reaching equilibrium in a reasonable time at low temperatures. Therefore, the increasing sorption amount and hysteresis observed between 25 and 77 K indicate that more H<sub>2</sub> molecules can access the pore system at higher temperatures due to thermally induced gate opening of the two bottleneck windows. Identical phenomena are also observed in the D<sub>2</sub> sorption, shown in Figure S8. The slightly higher D<sub>2</sub> uptake in comparison to H<sub>2</sub> is mainly attributed to the higher diffusion rate and the higher heat of adsorption of D<sub>2</sub>. Generally, for both (H<sub>2</sub> and D<sub>2</sub>) isotherms, the stronger hysteresis at lower temperature, which decreases at higher *T*, clearly denotes a temperature-dependent diffusion limitation of the gas molecules penetrating the cavities of the structure through different apertures (bottlenecks). Moreover, the higher D<sub>2</sub> uptake with slightly weaker hysteresis (Figure S8) in comparison to H<sub>2</sub> in the temperature range of 40–77 K additionally implies a difference in the diffusion kinetics between the two isotopes.

This temperature-dependent gating effect can be ascribed to the thermal vibration of the flexible windows as gates in the framework. At sufficiently low temperatures, the aperture becomes inaccessible to H<sub>2</sub> molecules due to the overcompensation of the potential barrier to the kinetic energy of molecules at the aperture. The model has been similarly used by Fernandez et al.<sup>29</sup> to explain the increased Kr/Xe selectivity observed at low temperatures. These results imply that the flexibility observed in FMOFCu is only local (no structural change), in contrast to the most well known flexible

(breathing) frameworks (e.g., MIL-53),<sup>21</sup> which show a volume change of the framework. In situ neutron powder diffraction (NPD) experiments have been also carried out to identify the possible structure changes of FMOFCu. All diffraction data have been collected at 24 K under vacuum or after exposure at room temperature with D<sub>2</sub> (Figure S9). Although the statistics of the diffraction peaks are rather poor, the NPD pattern indicates no visible structural change in FMOFCu, which may support the local flexibility ascribed to thermal vibrations of CF<sub>3</sub> group at the pore aperture.

Owing to the unique local flexibility, the cryogenically hindered diffusion at the aperture can be exploited for KQS, which is a prerequisite for isotope separation. In order to verify the hydrogen isotope separation performance, as well as the preferred H<sub>2</sub> and D<sub>2</sub> adsorption sites in FMOFCu, cryogenic TDS measurements have been carried out by applying pure H<sub>2</sub> and D<sub>2</sub> atmospheres, respectively, under identical experimental conditions. The resulting TDS spectra obtained between 20 and 150 K are shown in Figure 3. The thermal desorption

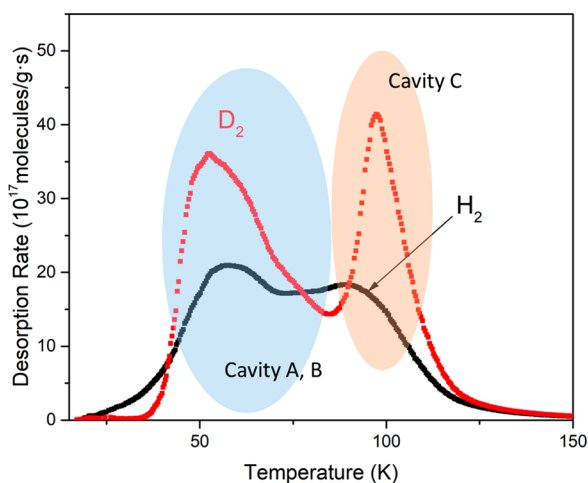


**Figure 3.** Pure gas H<sub>2</sub> (black) and D<sub>2</sub> (red) thermal desorption spectra of FMOFCu.

spectra of FMOFCu measured with H<sub>2</sub> and D<sub>2</sub> show two desorption maxima, which can be distinguishably assigned to the two different effective apertures of the alternating bimodal cavity and the hidden pocket. The first desorption peak for H<sub>2</sub> and D<sub>2</sub> appeared at ca. 55 K, while the second peak appeared at a rather high temperature of around 90–100 K. Note that the desorption maxima of the TDS spectra shift normally from weak to strong adsorption sites with rising temperatures<sup>38</sup> if no diffusion barrier exists. As there is no significantly strong sorption site (e.g., unsaturated open metal site) in the crystallographic structure of FMOFCu, these two distinguishable peaks can be attributed to two (3.6 and 2.5 Å) narrow windows which cause a strong diffusion barrier. Hence, the thermally activated aperture becomes more open with increasing temperature, and this gate-opening temperature may be different for the isotopes H<sub>2</sub> and D<sub>2</sub> due to quantum effects. Similar phenomena have been also observed for other gases (Ar, N<sub>2</sub>).<sup>39</sup> The area under the desorption peak is proportional to the desorbed amount of gas, which can be quantified with calibration<sup>40</sup> (see Supporting Information). The uptakes for H<sub>2</sub> and D<sub>2</sub> are determined to be 2.1 and 3.1 mmol/g, respectively. The lower H<sub>2</sub> uptake also implies a kinetic hindrance at the aperture, where H<sub>2</sub> encountered a

larger diffusion barrier in comparison to D<sub>2</sub> under identical conditions (pressure, temperature, and exposure time). Please note that such narrow windows producing a strong diffusion barrier lead to the desorption spectrum extending to a temperature of ca. 130 K for both isotopes. This is one of the rare examples exhibiting a high desorption temperature of physisorbed hydrogen in porous materials without the existence of open metal sites.

Encouraged by the difference of the desorbed amount between D<sub>2</sub> and H<sub>2</sub>, we investigated direct separation for an isotopic mixture. Owing to the favored D<sub>2</sub> sorption on the accessible internal surface, as well as faster diffusion of the heavier isotope into the aperture, higher selectivity in comparison to the D<sub>2</sub>/H<sub>2</sub> molar ratio from the pure gas experiments can be expected. Figure 4 shows the TDS spectra

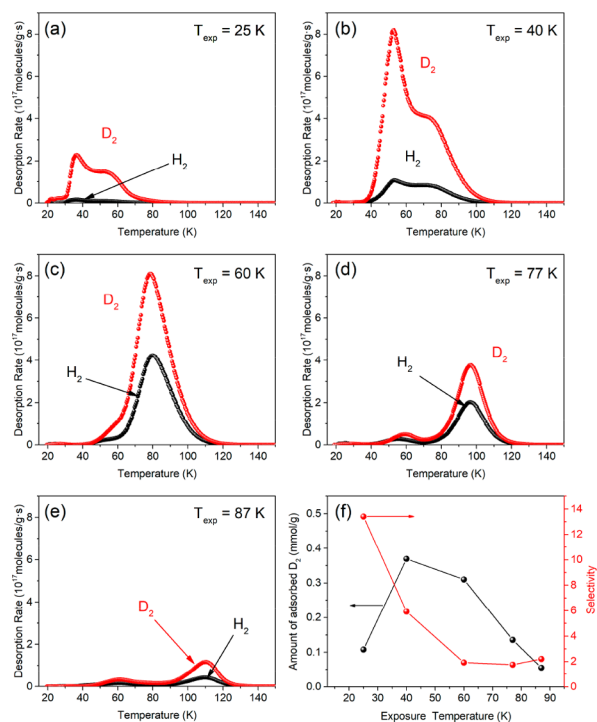


**Figure 4.** H<sub>2</sub> (black) and D<sub>2</sub> (red) thermal desorption spectra of a 10 mbar 1/1 H<sub>2</sub>/D<sub>2</sub> isotope mixture on FMOFCu for 10 min at various exposure temperatures ( $T_{\text{exp}}$ ): (a) 25 K; (b) 40 K; (c) 60 K; (d) 77 K; (e) 87 K. (f) The corresponding amount of adsorbed D<sub>2</sub> (black) and selectivity (red) as a function of  $T_{\text{exp}}$ .

collected after exposure of FMOFCu to a 10 mbar 1/1 H<sub>2</sub>/D<sub>2</sub> isotope mixture for 10 min at different exposure temperatures. The selectivity of D<sub>2</sub> over H<sub>2</sub> ( $S_{\text{D}_2/\text{H}_2}$ ) can be directly calculated from the integrated amount of the desorption peaks after calibration.<sup>41</sup> Figure 4f shows the D<sub>2</sub>/H<sub>2</sub> selectivity and its corresponding D<sub>2</sub> uptake as a function of exposure temperature ( $T_{\text{exp}}$  is approximately the temperature at which the isotope mixture is loaded). The total uptake in the nanopores increases with rising temperatures, exhibiting a maximum for the H<sub>2</sub> uptake at  $T_{\text{exp}} = 60$  K and D<sub>2</sub> uptake at  $T_{\text{exp}} = 40$  K before it decreases again until 87 K. Meanwhile, the selectivity decreases with increasing  $T_{\text{exp}}$ , exhibiting the highest value  $S_{\text{D}_2/\text{H}_2} = 14$  at 25 K. Normally, if different sorption sites exist inside porous media, the strongest site (high temperature desorption peak) is occupied first at very low loadings. Afterward, the weaker site is occupied at higher gas loadings,

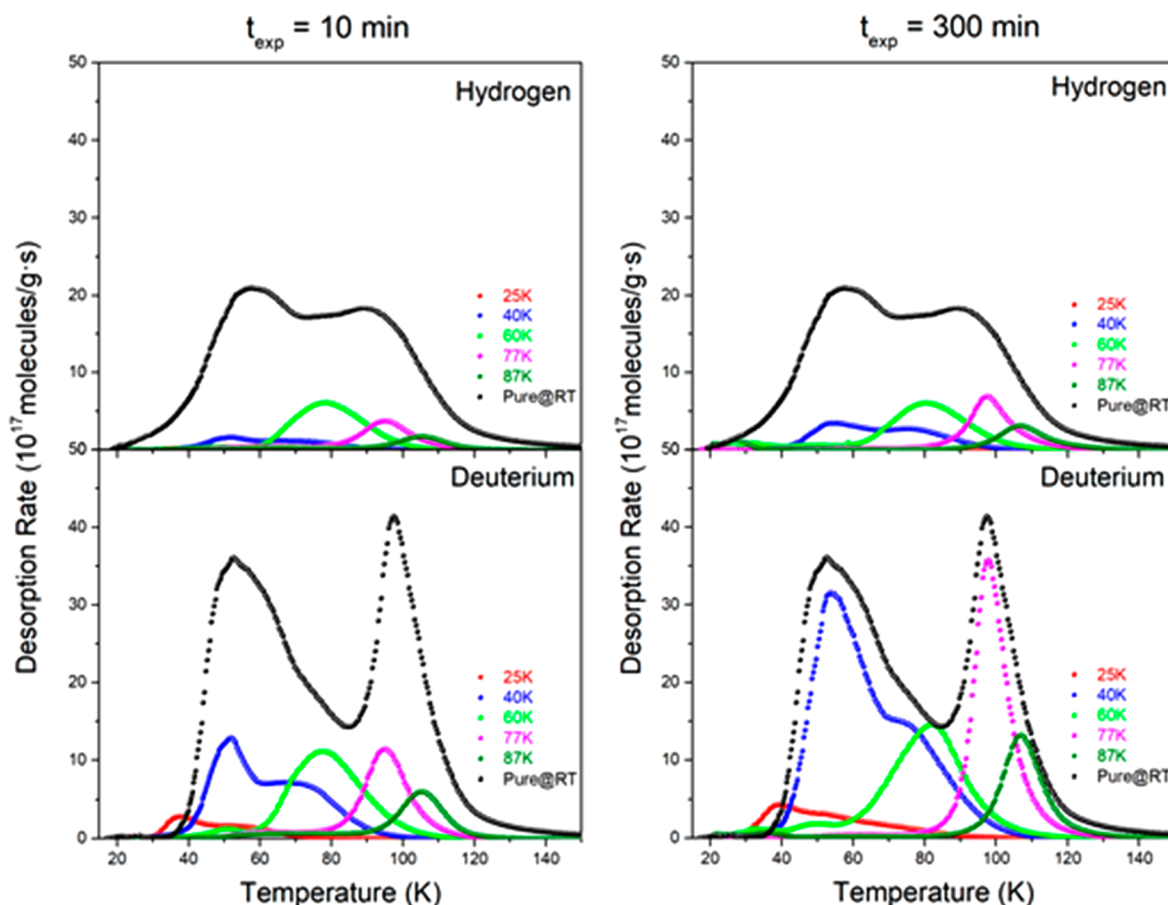


**Figure 5.** H<sub>2</sub> and D<sub>2</sub> thermal desorption spectra of a 50 mbar 1/1 H<sub>2</sub>/D<sub>2</sub> isotope mixture on FMOFCu for 10 and 300 min at various exposure temperatures ( $T_{\text{exp}}$ ): 25 K (red); 40 K (blue); 60 K (green); 77 K (magenta); 87 K (olive) and pure gas H<sub>2</sub> and D<sub>2</sub> thermal desorption spectra (black) for a comparison of accessible adsorption sites and gas uptake.

resulting in additional low-temperature desorption peaks. Namely, TDS spectra show typically a sequential filling from strong (higher desorption temperature) to weak adsorption sites (lower desorption temperature), exhibiting one, two, or multiple maxima. However, the H<sub>2</sub> and D<sub>2</sub> TDS spectra of FMOFCu in Figure 4 vary in shape and magnitude depending on  $T_{\text{exp}}$ , which is contrary to the typical sequential filling behavior of accessible sites with different binding strength. Interestingly, not only is the lowest uptake with highest selectivity observed for  $T_{\text{exp}} = 25$  K but also no desorption of any isotopes occurs above 70 K (Figure 4a), leading to an almost vanished third desorption peak. For  $T_{\text{exp}} > 60$  K, the second desorption peak in the spectrum becomes larger and the third peak appears simultaneously. The missing low-temperature peak (first desorption peak) is attributed to (1) the desorption of isotopes possessing sufficient kinetic energy to overcome a diffusion barrier to diffuse out of the channel during evacuation at  $T_{\text{exp}}$  and (2) local vibrations of the aperture at  $T_{\text{exp}}$ . These temperature-dependent TDS spectra are in agreement with the observation from pure gas isotherms, which is related to the temperature-triggered gate-opening behavior of the material.

For low exposure temperatures ( $T_{\text{exp}} = 25$  K), the isotope separation is mainly governed by the faster diffusion of D<sub>2</sub> through the 3.6 Å aperture (cavities A and B), while cavity C is still not accessible. As reported by Bhatia et al.,<sup>42</sup> the D<sub>2</sub> diffusivity gets significantly faster than H<sub>2</sub> below 50 K in carbon molecular sieve Takeda 3A, which has a pore aperture

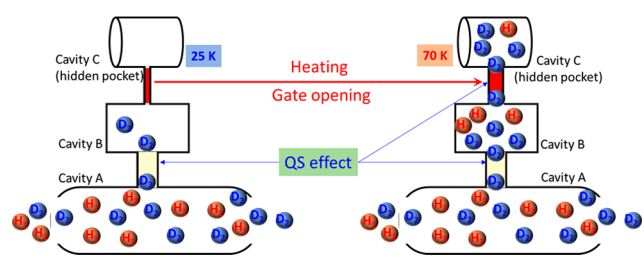
of 3.0 Å. Thus, the confined aperture of 3.6 Å at 25 K produces a strong diffusion barrier, allowing D<sub>2</sub> to preferentially penetrate into the cavities A and B, resulting in a high selectivity. On the other hand, this strong diffusion barrier leads to a rather small gas uptake within the exposure time (10 min). When  $T_{\text{exp}}$  increases to 40 K, the increasing isotope uptake with decreasing selectivity is related to the opening of the aperture by local vibrations and the sufficient kinetic energy of the molecule, where the accessibility of both isotopes is enhanced. For  $T_{\text{exp}} > 60$  K, the 2.5 Å aperture connecting for cavity C opens thermally activated and the third desorption peak appears.

Despite such low uptake and selectivity, after exposure at  $T_{\text{exp}} = 77$  and 87 K to an isotope mixture the desorption maxima are centered at 96 and 110 K, respectively, which is a rare case exhibiting such high desorption temperatures without the existence of strong adsorption sites. In general, desorption peaks at such high temperatures indicate the existence of strong binding sites, such as the open metal sites in MOF-74.<sup>40</sup> Although there is a difference in total uptake, it is still interesting to compare the high-temperature desorption spectra (60, 77, and 87 K) of FMOFCu and MOF-74-Ni (Figure S10). FMOFCu exhibits higher desorption maxima at all chosen exposure temperatures in comparison to MOF-74-Ni possessing unsaturated Ni sites. Since the isosteric heat of adsorption in FMOFCu was calculated to be 3–3.5 kJ/mol (Figure S11) using the Clausius–Clapeyron equation, this is clear evidence of the absence of any strong sorption site. Thus,

the size of the bottleneck aperture is temperature dependent and allows gas molecules to penetrate or leave the small cavity C only above this gate-opening temperature. When the system is cooled below the opening temperature under a gas atmosphere, the gas will be captured in the small cavity and can be only released by heating above the opening temperature. Therefore, this thermally triggered local flexibility is responsible for the high-temperature desorption peak. Introducing bottleneck apertures into the MOF pore structure results in a diffusion barrier for hydrogen, which drastically increases the desorption temperature to one comparable to or even higher than the desorption temperatures reached by open metal sites in other MOFs.

Since FMOFCu possesses a very narrow aperture, the adsorption process requires sufficient time to reach equilibrium. In order to reveal the dependence of isotope separation performance on exposure time ( $t_{\text{exp}}$ ) and temperature ( $T_{\text{exp}}$ ), TDS measurements have been performed by applying a 50 mbar 1/1 isotope mixture at 25–87 K for different  $t_{\text{exp}}$ . Figure 5 shows  $\text{H}_2$  and  $\text{D}_2$  TDS spectra at different  $T_{\text{exp}}$  for 10 and 300 min of exposure time. (For TDS spectra collected at other  $t_{\text{exp}}$  (60, 120 min), see Figure S12.) Note that one mixture measurement of TDS at a given  $t_{\text{exp}}$  and  $T_{\text{exp}}$  provides each hydrogen and deuterium signal individually, and the hydrogen (top in Figure 5) and deuterium (bottom in Figure 5) signals are presented separately to show the dependence of time and temperature. All black curves in Figure 5 imply the pure gas TDS (loading at room temperature and then cooling below 20 K; Figure 3), in which all adsorption sites are assumed to be accessible for both isotopes. It is clear that 10 min of exposure time (Figure 5 left) is not enough to reach an equilibrium, while  $t_{\text{exp}}$  for 300 min (Figure 5 right) at a 50 mbar mixture exposure, the sum of all  $\text{D}_2$  spectra collected at different  $T_{\text{exp}} = 25\text{--}87\text{ K}$  has as an envelope the pure gas TDS for room temperature exposure. This successive filling of the different cavities by increasing the exposure temperature is illustrated in Scheme 1. At low exposure temperatures up to 40 K only

**Scheme 1. Schematic View of the Trimodal Structure of FMOFCu**



cavities A and B are accessible for gas molecules and the bottleneck aperture to cavity C is still closed. At higher exposure temperatures this small aperture opens thermally activated and gas can penetrate into cavity C. Thus, the high selectivity is initially observed at  $T_{\text{exp}} = 25\text{ K}$  with low uptake due to the barely open aperture. Then, the selectivity decreases with temperature due to opening the aperture but increases again for 77 and 87 K in comparison to 60 K (Figure 4f), since the aperture of cavity C is opening and acting as another sieve (Scheme 1).

## CONCLUSIONS

In summary, we experimentally investigated a partially fluorinated MOF, FMOFCu, for efficient hydrogen isotope separation. The framework possesses a trimodal pore structure, where the alternating large tubular cavities connected with small windows are accompanied by the hidden pockets blocked by fluorinated windows. This trimodal structure exhibits a unique feature of temperature-triggered gate opening. When this gate opening is exploited, the highest selectivity of 14 at 25 K can be observed on the basis of the optimal KQS effect generated by the proper pore aperture size of the small windows. The additional presence of a hidden cavity in the FMOFCu structure blocked by a small bottleneck aperture, which opens on thermal activation, offers a newly accessible inner surface to increase the adsorption of hydrogen isotopes inside the framework and a second narrow channel for quantum sieving. This leads to a desorption temperature of over 100 K, comparable to that of strong adsorption sites, even though none are present in FMOFCu. Furthermore, a selectivity between 3 and 4 is still achieved at exposure temperatures of 77 and 87 K, showing the potential of this material for isotope separation above liquid nitrogen temperature.

## ASSOCIATED CONTENT

### Supporting Information

The Supporting Information is available free of charge on the ACS Publications Web site at DOI: The Supporting Information is available free of charge at <https://pubs.acs.org/doi/10.1021/jacs.9b10268>.

Experimental details, SEM data, TG data, XRD data, FT-IR spectra, BET surface areas, gas adsorption isotherms, NPD data, and TDS spectra (PDF)

Crystallographic data (CIF)

CheckCIF report (PDF)

## AUTHOR INFORMATION

### Corresponding Authors

\*E-mail for K.C.: [kmchoi@sookmyung.ac.kr](mailto:kmchoi@sookmyung.ac.kr).

\*E-mail for M.H.: [hirscher@is.mpg.de](mailto:hirscher@is.mpg.de).

\*E-mail for H.O.: [oh@gntech.ac.kr](mailto:oh@gntech.ac.kr).

### ORCID

Minyoung Yoon: 0000-0001-7436-6273

Kyungmin Choi: 0000-0001-7181-902X

Michael Hirscher: 0000-0002-3143-2119

Hyunchul Oh: 0000-0001-6258-0002

### Author Contributions

◇L.Z. and S.J. contributed equally.

### Notes

The authors declare no competing financial interest.

## ACKNOWLEDGMENTS

This work was supported by a National Research Foundation of Korea (NRF) Grant funded by the Korean Government (MSI) (No. 2019R1A2C2005162, No. 2019K1A3A7A09094067, No. 2019R1A2C4069764). The single-crystal X-ray diffraction experiment at the PLS-II, 2D-SMC beamline was supported by MSIT and POSTECH. The neutron source BER II in HZB is gratefully acknowledged for the allocation of neutron scattering beamtime on E9 beamlines and for travel grants.

## REFERENCES

- (1) Kim, J. Y.; Balderas-Xicohténcatl, R.; Zhang, L.; Kang, S. G.; Hirscher, M.; Oh, H.; Moon, H. R. Exploiting diffusion barrier and chemical affinity of metal-organic frameworks for efficient hydrogen isotope separation. *J. Am. Chem. Soc.* **2017**, *139* (42), 15135–15141.
- (2) Greenwood, N. N.; Earnshaw, A. *Chemistry of the Elements*. Elsevier: 2012.
- (3) Rae, H. K. *Separation of hydrogen isotopes*; American Chemical Society: Washington, DC, 1978.
- (4) Oh, H.; Hirscher, M. Quantum sieving for separation of hydrogen isotopes using MOFs. *Eur. J. Inorg. Chem.* **2016**, *2016* (27), 4278–4289.
- (5) Beenakker, J.; Borman, V.; Krylov, S. Y. Molecular transport in subnanometer pores: zero-point energy, reduced dimensionality and quantum sieving. *Chem. Phys. Lett.* **1995**, *232* (4), 379–382.
- (6) Krkljus, I.; Steriotis, T.; Charalambopoulou, G.; Gotzias, A.; Hirscher, M. H<sub>2</sub>/D<sub>2</sub> adsorption and desorption studies on carbon molecular sieves with different pore structures. *Carbon* **2013**, *57*, 239–247.
- (7) Kowalczyk, P.; Gauden, P. A.; Terzyk, A. P.; Furmaniak, S. Impact of the carbon pore size and topology on the equilibrium quantum sieving of hydrogen isotopes at zero coverage and finite pressures. *J. Phys.: Condens. Matter* **2009**, *21* (14), 144210.
- (8) Xiong, R.; Xicohténcatl, R. B.; Zhang, L.; Li, P.; Yao, Y.; Sang, G.; Chen, C.; Tang, T.; Luo, D.; Hirscher, M. Thermodynamics, kinetics and selectivity of H<sub>2</sub> and D<sub>2</sub> on zeolite 5A below 77K. *Microporous Mesoporous Mater.* **2018**, *264*, 22–27.
- (9) Oh, H.; Kalidindi, S. B.; Um, Y.; Bureekaew, S.; Schmid, R.; Fischer, R. A.; Hirscher, M. A cryogenically flexible covalent organic framework for efficient hydrogen isotope separation by quantum sieving. *Angew. Chem., Int. Ed.* **2013**, *52* (50), 13219–13222.
- (10) Savchenko, I.; Mavrandonakis, A.; Heine, T.; Oh, H.; Teufel, J.; Hirscher, M. Hydrogen isotope separation in metal-organic frameworks: Kinetic or chemical affinity quantum-sieving? *Microporous Mesoporous Mater.* **2015**, *216*, 133–137.
- (11) Mondal, S. S.; Kreuzer, A.; Behrens, K.; Schütz, G.; Holdt, H. J.; Hirscher, M. Systematic Experimental Study on Quantum Sieving of Hydrogen Isotopes in Metal-Amide-Imidazolate Frameworks with narrow 1-D Channels. *ChemPhysChem* **2019**, *20* (10), 1311–1315.
- (12) Cai, J.; Xing, Y.; Zhao, X. Quantum sieving: feasibility and challenges for the separation of hydrogen isotopes in nanoporous materials. *RSC Adv.* **2012**, *2* (23), 8579–8586.
- (13) Liu, D.; Wang, W.; Mi, J.; Zhong, C.; Yang, Q.; Wu, D. Quantum Sieving in Metal-Organic Frameworks: A Computational Study. *Ind. Eng. Chem. Res.* **2012**, *51* (1), 434–442.
- (14) Weinrauch, I.; Savchenko, I.; Denysenko, D.; Souliou, S.; Kim, H.; Le Tacon, M.; Daemen, L. L.; Cheng, Y.; Mavrandonakis, A.; Ramirez-Cuesta, A. Capture of heavy hydrogen isotopes in a metal-organic framework with active Cu (I) sites. *Nat. Commun.* **2017**, *8*, 14496.
- (15) Chen, B.; Zhao, X.; Putkham, A.; Hong, K.; Lobkovsky, E. B.; Hurtado, E. J.; Fletcher, A. J.; Thomas, K. M. Surface interactions and quantum kinetic molecular sieving for H<sub>2</sub> and D<sub>2</sub> adsorption on a mixed metal-organic framework material. *J. Am. Chem. Soc.* **2008**, *130* (20), 6411–6423.
- (16) Oh, H.; Park, K. S.; Kalidindi, S. B.; Fischer, R. A.; Hirscher, M. Quantum cryo-sieving for hydrogen isotope separation in microporous frameworks: an experimental study on the correlation between effective quantum sieving and pore size. *J. Mater. Chem. A* **2013**, *1* (10), 3244–3248.
- (17) Horike, S.; Shimomura, S.; Kitagawa, S. Soft porous crystals. *Nat. Chem.* **2009**, *1* (9), 695.
- (18) Tanaka, D.; Nakagawa, K.; Higuchi, M.; Horike, S.; Kubota, Y.; Kobayashi, T. C.; Takata, M.; Kitagawa, S. Kinetic Gate-Opening Process in a Flexible Porous Coordination Polymer. *Angew. Chem., Int. Ed.* **2008**, *47* (21), 3914–3918.
- (19) Lin, Z.-J.; Lü, J.; Hong, M.; Cao, R. Metal-organic frameworks based on flexible ligands (FL-MOFs): structures and applications. *Chem. Soc. Rev.* **2014**, *43* (16), 5867–5895.
- (20) Schneemann, A.; Bon, V.; Schwedler, I.; Senkovska, I.; Kaskel, S.; Fischer, R. A. Flexible metal-organic frameworks. *Chem. Soc. Rev.* **2014**, *43* (16), 6062–6096.
- (21) Kim, J. Y.; Zhang, L.; Balderas-Xicohténcatl, R.; Park, J.; Hirscher, M.; Moon, H. R.; Oh, H. Selective hydrogen isotope separation via breathing transition in MIL-53 (Al). *J. Am. Chem. Soc.* **2017**, *139* (49), 17743–17746.
- (22) Ribeiro, R. P.; Camacho, B. C.; Lyubchik, A.; Esteves, I. A.; Cruz, F. J.; Mota, J. P. Experimental and computational study of ethane and ethylene adsorption in the MIL-53 (Al) metal organic framework. *Microporous Mesoporous Mater.* **2016**, *230*, 154–165.
- (23) Teufel, J.; Oh, H.; Hirscher, M.; Wahiduzzaman, M.; Zhechkov, L.; Kuc, A.; Heine, T.; Denysenko, D.; Volkmer, D. MFU-4A Metal-Organic Framework for Highly Effective H<sub>2</sub>/D<sub>2</sub> Separation. *Adv. Mater.* **2013**, *25* (4), 635–639.
- (24) Noro, S.-i.; Nakamura, T. Fluorine-functionalized metal-organic frameworks and porous coordination polymers. *NPG Asia Mater.* **2017**, *9* (9), No. e433.
- (25) Hulvey, Z.; Falcao, E. H.; Eckert, J.; Cheetham, A. K. Enhanced H<sub>2</sub> adsorption enthalpy in the low-surface area, partially fluorinated coordination polymer Zn 5 (triazole) 6 (tetrafluoroterephthalate) 2 (H<sub>2</sub>O) 2 · 4H<sub>2</sub>O. *J. Mater. Chem.* **2009**, *19* (25), 4307–4309.
- (26) Zhang, D.-S.; Chang, Z.; Li, Y.-F.; Jiang, Z.-Y.; Xuan, Z.-H.; Zhang, Y.-H.; Li, J.-R.; Chen, Q.; Hu, T.-L.; Bu, X.-H. Fluorous metal-organic frameworks with enhanced stability and high H<sub>2</sub>/CO<sub>2</sub> storage capacities. *Sci. Rep.* **2013**, *3*, 3312.
- (27) Yang, C.; Wang, X.; Omary, M. A. Crystallographic observation of dynamic gas adsorption sites and thermal expansion in a breathable fluorinated metal-organic framework. *Angew. Chem., Int. Ed.* **2009**, *48* (14), 2500–2505.
- (28) Pan, L.; Sander, M. B.; Huang, X.; Li, J.; Smith, M.; Bittner, E.; Bockrath, B.; Johnson, J. K. Microporous metal organic materials: promising candidates as sorbents for hydrogen storage. *J. Am. Chem. Soc.* **2004**, *126* (5), 1308–1309.
- (29) Fernandez, C. A.; Liu, J.; Thallapally, P. K.; Strachan, D. M. Switching Kr/Xe selectivity with temperature in a metal-organic framework. *J. Am. Chem. Soc.* **2012**, *134* (22), 9046–9049.
- (30) Liu, J.; Fernandez, C. A.; Martin, P. F.; Thallapally, P. K.; Strachan, D. M. A two-column method for the separation of Kr and Xe from process off-gases. *Ind. Eng. Chem. Res.* **2014**, *53* (32), 12893–12899.
- (31) Arvai, A. J.; Nielsen, C. *ADSC Quantum-210 ADX Program*; Area Detector System Corporation: Poway, CA, USA, 1983.
- (32) Otwinowski, Z.; Minor, W. [20] Processing of X-ray diffraction data collected in oscillation mode. In *Methods in enzymology*; Elsevier: 1997; Vol. 276, pp 307–326.
- (33) Sheldrick, G. M. SHELXT-Integrated space-group and crystal-structure determination. *Acta Crystallogr., Sect. A: Found. Adv.* **2015**, *71* (1), 3–8.
- (34) Sheldrick, G. M. Crystal structure refinement with SHELXL. *Acta Crystallogr., Sect. C: Struct. Chem.* **2015**, *71* (1), 3–8.
- (35) Dybtssev, D. N.; Chun, H.; Kim, K. Rigid and flexible: a highly porous metal-organic framework with unusual guest-dependent dynamic behavior. *Angew. Chem., Int. Ed.* **2004**, *43* (38), 5033–5036.
- (36) Fernandez, C. A.; Thallapally, P. K.; Motkuri, R. K.; Nune, S. K.; Sumrak, J. C.; Tian, J.; Liu, J. Gas-induced expansion and contraction of a fluorinated metal-organic framework. *Cryst. Growth Des.* **2010**, *10* (3), 1037–1039.
- (37) Macrae, C. F.; Bruno, I. J.; Chisholm, J. A.; Edgington, P. R.; McCabe, P.; Pidcock, E.; Rodriguez-Monge, L.; Taylor, R.; Streek, J. v. d.; Wood, P. A. Mercury CSD 2.0-new features for the visualization and investigation of crystal structures. *J. Appl. Crystallogr.* **2008**, *41* (2), 466–470.
- (38) Panella, B.; Hönes, K.; Müller, U.; Trukhan, N.; Schubert, M.; Pütter, H.; Hirscher, M. Desorption studies of hydrogen in metal-organic frameworks. *Angew. Chem., Int. Ed.* **2008**, *47* (11), 2138–2142.
- (39) Kim, H.; Samsonenko, D. G.; Yoon, M.; Yoon, J. W.; Hwang, Y. K.; Chang, J.-S.; Kim, K. Temperature-triggered gate opening for gas

adsorption in microporous manganese formate. *Chem. Commun.* **2008**, No. 39, 4697–4699.

(40) Oh, H.; Savchenko, I.; Mavrandonakis, A.; Heine, T.; Hirscher, M. Highly effective hydrogen isotope separation in nanoporous metal-organic frameworks with open metal sites: direct measurement and theoretical analysis. *ACS Nano* **2014**, *8* (1), 761–770.

(41) Panella, B.; Hirscher, M.; Ludescher, B. Low-temperature thermal-desorption mass spectroscopy applied to investigate the hydrogen adsorption on porous materials. *Microporous Mesoporous Mater.* **2007**, *103* (1–3), 230–234.

(42) Nguyen, T. X.; Jobic, H.; Bhatia, S. K. Microscopic observation of kinetic molecular sieving of hydrogen isotopes in a nanoporous material. *Phys. Rev. Lett.* **2010**, *105* (8), 085901.